PROCEEDINGS, 50th Workshop on Geothermal Reservoir Engineering
Stanford University, Stanford, California, February 10-12, 2025
SGP-TR-229

Preliminary Analysis of Results from the Utah FORGE Project

Mark W. McClure

ResFrac Corporation

mark@resfrac.com

Keywords: Utah FORGE, EGS, stimulation, tracer testing, crosswell fiber

ABSTRACT

Over the past year, the Utah FORGE project has performed a series of hydraulic stimulations and circulation tests. A diversity of data has been gathered, which is still in the process of being analyzed and published. This paper provides preliminary analysis, which is drawn from the data that has been presented publicly to-date. Key observations are: (a) plug and perf stimulation with proppant has delivered dramatically improved EGS performance relative to conventional EGS designs, (b) stimulations without proppant have been ineffective, (c) field tests not found evidence of significant shear stimulation of natural fractures, (d) a larger-scale fault/fracture zone appears to have affected fracture morphology in at least one stage, diverting fracture propagation, (e) flow uniformity along the 16(A) well is adequate but not ideal, (f) geologic variability is substantial, complicating efforts to evaluate the impact of the different stimulation designs that were trialed along the lateral, and (g) tracer tests indicate a surprisingly large swept volume, suggesting that: (i) flow is occurring through a reasonably large number of flowing fractures, and (ii) proppant has likely created a larger than expected propped fracture surface area. Several recent papers and presentations have proposed interpretations of the data that are, in part, inconsistent with the conclusions listed above. This paper briefly notes those analyses and provides critical analysis.

1. INTRODUCTION

1.1 Background

In 2024, the Utah FORGE project executed a series of hydraulic stimulations and circulation tests, with a sustained production rate of 26 kg/s across roughly 1000 ft of stimulated lateral (Utah FORGE, 2024a,b; England et al., 2025). Because a full-scale system would utilize 5000-8000 ft of lateral and involve flow in multiple directions to different wells, the results suggest that circulation rates greater than 100 kg/s should be possible for a full-scale system. In fact, the nearby Project Cape operated by Fervo Energy has achieved flow rates of 93-121 kg/s during circulation (Norbeck and Latimer, 2023; Norbeck et al., 2024). Overall, these projects validate that multistage plug and perf completion achieves dramatically improved performance, relative to classical EGS designs.

1.2 Summary of relevant FORGE operations

Table 1 provides a timeline of key events at the FORGE project (Moore et al., 2023; Utah FORGE, 2024a). Well 16(A) was drilled in Q1 2021. It is deviated at 65° from vertical to an MD of 10,987 ft, in the approximate direction of the minimum principal stress. The total vertical depth is 8561 ft, with an estimated bottomhole temperature of approximately 429°F (Moore et al., 2023). Three proppantless stimulation stages were performed in 16(A) in April 2022. Well 16(B) is drilled to similar depth, with a lateral parallel to the 16(A) about 330 ft directly above, with similar inclination and azimuth. Well 16(B) was drilled and partially cored through the SRV of the initial 16(A) stimulations, as identified from microseismic. An openhole section was left towards the toe of 16(B), in order to intersect the fractures created by the previous 16(A) stimulation. In July 2023, circulation tests were performed between 16(A) and 16(B). As discussed in Section 2.2, the circulation rate was during this test was very low.

From March to April 2024, propped stimulation treatments were performed in 16(B) and 16(A). The original three stages of 16(A) were restimulated with proppant (Stage 3R), and then seven news stages were pumped (Stages 4-10). Stage 10 was not originally planned. However, maximum wellhead constraints were reached during Stages 6 and 7 (8000 psi), making it impossible to pump the designed job. As a result, Stage 10 was added at the end. Well 16(B) was subsequently stimulated, albeit with much smaller volume of fluid and proppant, in five fracturing stages. Subsequently, a nine-hour circulation test was performed in April 2024, and a 30-day circulation test was performed in August and September 2024. These circulation tests achieved much higher rate than the previous tests in July 2023. All circulation tests used the underlying 16(A) well as the injector.

Table 1: Timeline of key events at FORGE (Moore et al., 2023; Utah FORGE, 2024).

Q1 2021	Drilling of Well 16(A)
April 2022	Three-stage proppantless stimulation in 16(A)
May-July 2023	Drilling of Well 16(B)
July 2023	Circulation tests between 16(A) and 16(B)
March-April 2024	Propped stimulation of Stages 3R to 10 in 16(A) and smaller-volume stimulation Stages 1 to 5 in 16(B)
April 2024	Nine-hour circulation test between 16(A) and 16(B)
Aug-Sept 2024	30-day circulation test between 16(A) and 16(B)

Table 2: The fracture design 'as pumped' in the Well 16(A) (England, 2024; England et al., 2025).

Stage Name	Number of Clusters	Fluid Type	Fluid Volume (bbl)	Pump Rate (bpm)	100-mesh Prop Volume (lb_m)	40/70-mesh Prop Volume (lb_m)	30/80-mesh OmniProp (lb_m)	Comments
Stage 3R	2 + OH	Slickwater	10,318	50	136,260	199,300	N/A	
Stage 4	1	Slickwater	5,263	35 (Avg = 29)	54,920	77,700	N/A	
Stage 5	1	XL CMHPG	4,537	35 (Avg = 27)	55,680	81,200	N/A	
Stage 6A	1	Slickwater	1,516	11.7 (Avg = 7.9)	0	0	0	Surface pressure too high to start prop.
Stage 6B	2	Slickwater	1,796	16.4 (Avg = 10.4)	0	0	0	Perf additional 3 ft zone. Surface pressure still too high to start prop.
Stage 7	3	XL CMHPG	12,596	39 (Avg = 23)	0	0	N/A	Surface pressure too high to start prop.
Stage 8	8	XL CMHPG	35,295	80 (Avg = 71)	439,500	642,000	N/A	
Stage 9	8	Slickwater	27,237	80 (Avg = 72)	445,260	285,372	N/A	
Stage 10	1	Slickwater	4,550	35 (Avg = 29)	54,600	79,800	4,000	Repeat of Stage 6 with ULWP.
Circulation Test	All Zones	Slickwater	7,285	16.5 (Avg = 14)	N/A	N/A	N/A	Only able to pump 16 bpm max and had to reduce rate to stay below Shmin. Final rate of 12.5 bpm.

2. KEY OBSERVATIONS AND DISCUSSION

2.1 Overall performance of plug and perf fracturing with proppant for EGS

2.1.1 Overall flow rate

The goal of EGS stimulation is to achieve a high flow rate (ideally, greater than 100 kg/s), with flow distributed across a large fracture surface area. Traditionally, EGS wells have been drilled as vertical or subvertical and stimulated in a single openhole stage without proppant. Few, if any, of these projects have achieved target rates or fracture surface area (Tester, 2006). Recent EGS wells have used propped plug and perf completion along horizontal laterals (Norbeck and Latimer, 2023; Norbeck et al., 2024; Utah FORGE, 2024a,b). These projects have achieved much greater flow rates than previous EGS projects.

Like the projects from Norbeck and Latimer (2023) and Norbeck et al. (2024), the FORGE project has used propped plug and perf stimulation. Consistent with their results, this design has yielded strong circulation rates. During a 30-day circulation test, a sustained production rate of 28 kg/s was achieved (Figure 1). This rate is high by historic EGS standards, even though only 1000 ft of lateral have been stimulated to-date. Horizontal laterals in shale are typically 10,000-20,000 ft in length. Recent commercial EGS laterals have been 3000-6000 ft in length (Norbeck and Latimer, 2023; Norbeck et al., 2024). Therefore, the achievement of 28 kg/s from only 1000 ft of lateral is a positive result, suggesting that much higher flow rates will be possible with longer laterals. In fact, the nearby Project Cape wells have demonstrated flow rates in excess of 100 kg/s (Norbeck et al., 2024).

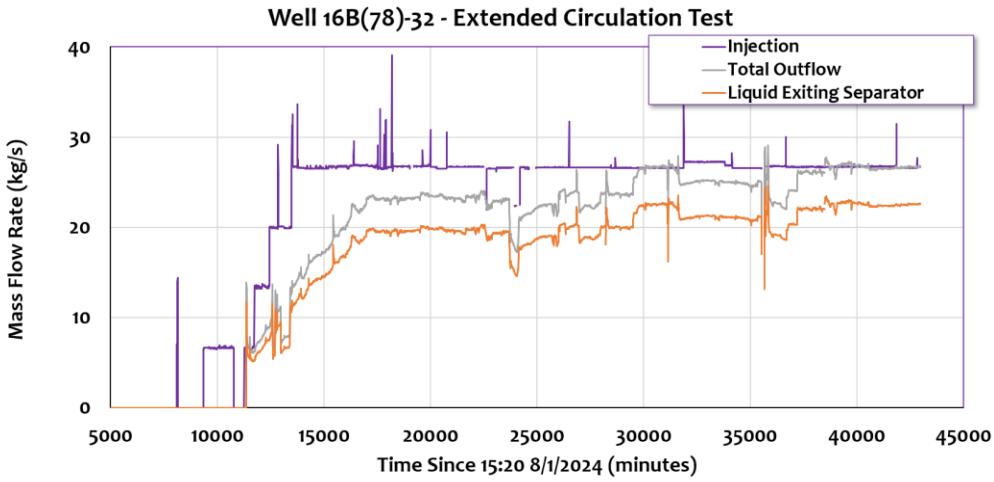

Figure 1: Injection and production rate versus time during the 30-day circulation test at FORGE from August to September 2024 (John McLennan, personal communication; Utah FORGE, 2024b).

2.1.2 Uniformity of flow

Flow uniformity is a key metric that we can use to evaluate the performance of an EGS. Designs with greater uniformity will have better thermal longevity. Traditional EGS designs have tended to suffer flow localization, with only a small number of flowing fracture pathways (Evans et al., 2005; Baria et al., 2005; Tenma et al., 2008). With plug and perf multistage completion, the hope has been that flow will be more uniform, because the combination of zonal isolation and limited-entry perforation pressure drop would generate a large number of relatively similar propped fractures (Glauser et al., 2013; Shiozawa and McClure, 2014). In fact, production logs from the recent Fervo Project Red show a relatively uniform distribution of flow (Norbeck and Latimer, 2023).

In the FORGE wells, results are mixed regarding the uniformity of flow. A challenge for interpretation is that every stage was stimulated with a different design. Clusters per stage varied from 1, 2, 4, and 8. Fluid types were mixed – some stages used slickwater and other used a much more viscous crosslinked CMHPG system. However, on a per-cluster basis, the volume of fluid and proppant pumped in each stage was relatively consistent.

In addition to the variability in frac design, there appears to be substantial geologic variability along the laterals. For example, Stages 6 (2 clusters) and 7 (4 clusters) required excessive surface pressure and could not be effectively stimulated. Evidently, this was caused by variability in either stress or rock strength. Core from the 16(B) shows that granitic rock intermixes with gneiss along the laterals (Jones et al., 2025).

During the nine-hour circulation test in April 2024, a spinner log was run in the 16(A) well. The results are shown in Figure 2. A spinner log was run again during the 30-day flow test. The results are shown in Figure 3. Flow rates are variable by stage, but the stages had variable number of perforation clusters and fluid and proppant volume. Therefore, we should primarily focus on uniformity by perforation cluster, rather than by stage. It was not possible to run the PLT log to the bottom of the hole, and so total fluid from the toe-side stages is aggregated.

During the April 2024 flow test, no more than 12% of flow was measured from any cluster. Stages 8 and 9 flowed the most, consistent with expectation since they had the most perforation clusters and injected the largest volume of proppant. Stage 9 took moderately more flow than Stage 8.

The results were surprisingly different during the August test (Figure 3). In this test, Stage 8 accepted substantially more flow than Stage 9. Stages 6 and 7 took negligible flow, which is unsurprising because these were the stages where injection pressures were excessively high and the job could not be pumped as designed. Stage 10 took a much higher proportion of flow in this test, 25.8%. This is concerning because Stage 10 had only a single perforation cluster. It is undesirable that so much flow would be flowing from a single perforation cluster. However, complicating this picture, the heel-side stage in the production well 16(B) did not accept a disproportionate amount of flow.

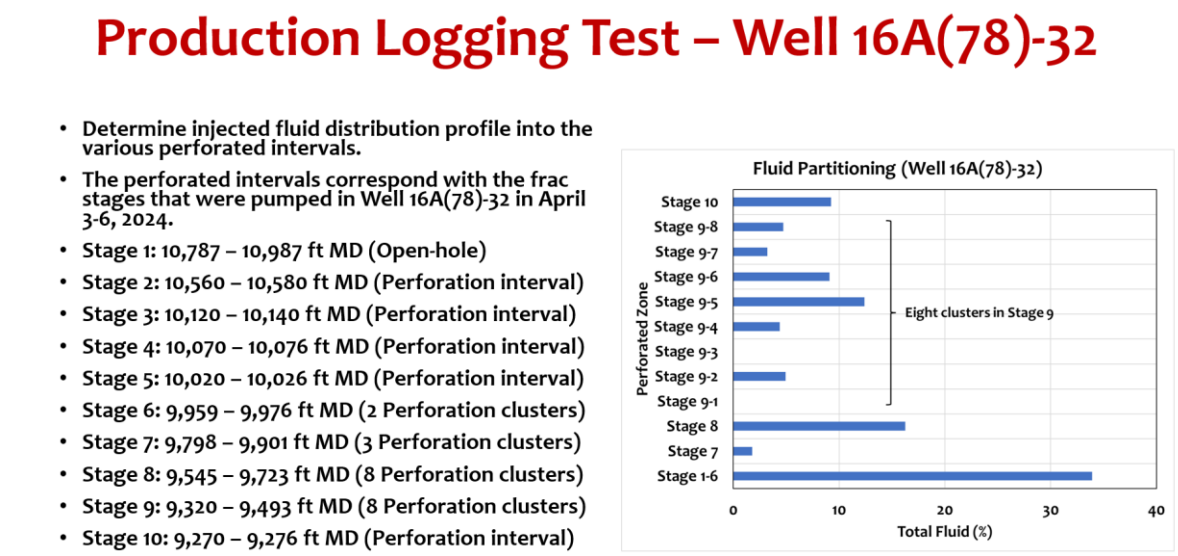

Figure 2: Production log flow distribution within the 16(A) well during circulation between the 16(A) and 16(B) wells during the 9-hour test in April 2024 (figures are reproduced from England, 2024).

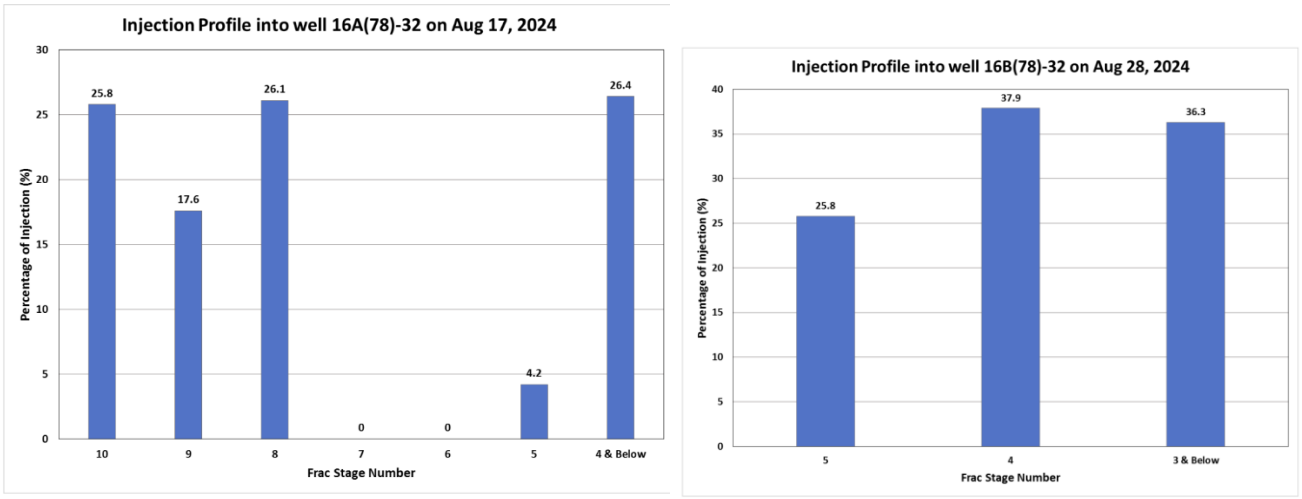

Figure 3: Production log flow distribution within the 16(A) well during circulation between the 16(A) and 16(B) wells during the 30-day test in August 2024 (figures are reproduced from England, 2024).

Overall, these results are adequate, but not as good as might be hoped. It is possible that changes in engineering parameters – such as perforation design and wellhead equipment – might have been able to reduce the observed variability. For example, more extreme limited-entry perforation design could have been employed to elevate injection pressure and potentially reduce the fraction of clusters that did not break down (Weddle et al., 2018).

It is not optimal for uniformity that different frac designs were used in every stage. It is difficult to assess whether the differences in flow are caused by changes in frac design or geology. The data has too much random variability to make generalizations based on such a small number of stages.

2.2 Shear stimulation and the impact of injecting proppant

In April 2022, three unpropped stimulation stages were performed in the 16(A) well (Table 1). Subsequently, the 16(B) well was drilled. 16(B) was completed with an openhole section at the toe, overlapping with the microseismic clouds created around the 16(A) well during the prior stimulation. When circulation was attempted between the wells in July 2023, the production rate was extremely low. Figure 4 (reproduced from Xing et al., 2024) shows pressures and rates from the circulation test.

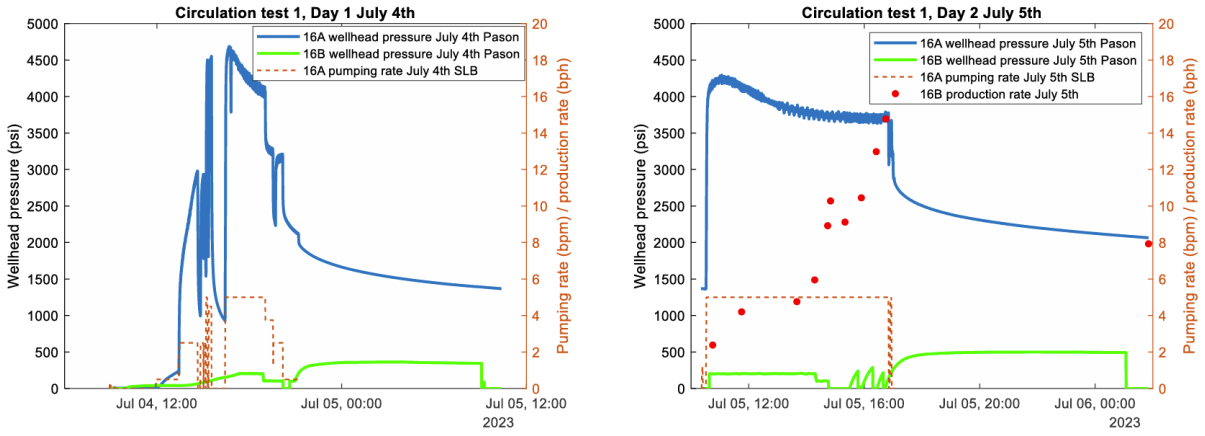

(a) **(b)**

Figure 4: WHP and rate of Wells 16(A) and 16(B) during the July 2023 circulation test. Figure is reproduced from Xing et al. (2024).

Initially, injection was performed into 16(A) at about 2.5 bpm (6.6 kg/s). The WHP of 16(A) increased rapidly. When rate was stepped up to 5 bpm (13 kg/s), the pressure increased rapidly to reach the minimum principal stress and then plateaued. In general, a plateauing of injection pressure occurs when BHP exceeds the minimum principal stress because the mechanical opening of new or preexisting fractures causes a large, reversible increase in fracture conductivity (Zoback, 2007). In practical application, injection with BHP above Shmin would probably not be performed during long-term EGS circulation because of the likelihood of excessive fluid loss due to fracture propagation and because of the increased likelihood of nonuniform flow between the fractures.

Even after the 16(A) BHP was increased above the jacking pressure at 5 bpm, the production rate in the 16(B) remained extremely low. The right panel of Figure 4 shows that after around 8 hours of injection, the production rate had increased to 16 barrels per hour, or 0.27 bpm (0.7 kg/s). The contrast in production rate in circulation tests following the propped (Figure 1) and unpropped (Figure 4) stimulations is stark, even though the July 2023 circulation tests after the unpropped fracture stimulations had an advantage because they were performed with BHP *above* Shmin.

To test for evidence of shear stimulation, a specialized injection sequence was used prior to the start of the first stimulation stage of the April 2022 stimulation of 16(A). This stage was performed in the openhole section at the toe of the well. The injection rate was controlled to bring the BHP close to the magnitude of Shmin, but to not exceed it. At a rate of 20 gpm (0.5 bpm), WHP reached 3250 psi, roughly 750 psi below where breakdown and fracture opening/closure were observed in subsequent tests (Figure 5; Utah FORGE, 2023). Injection pressure plateaued, perhaps indicating a limited amount of injectivity enhancement. Nevertheless, the overall injectivity remained very low, and microseismicity was not observed. Subsequently, when high-rate injection was performed with BHP above Shmin, microseismicity became widespread (Utah FORGE, 2023).

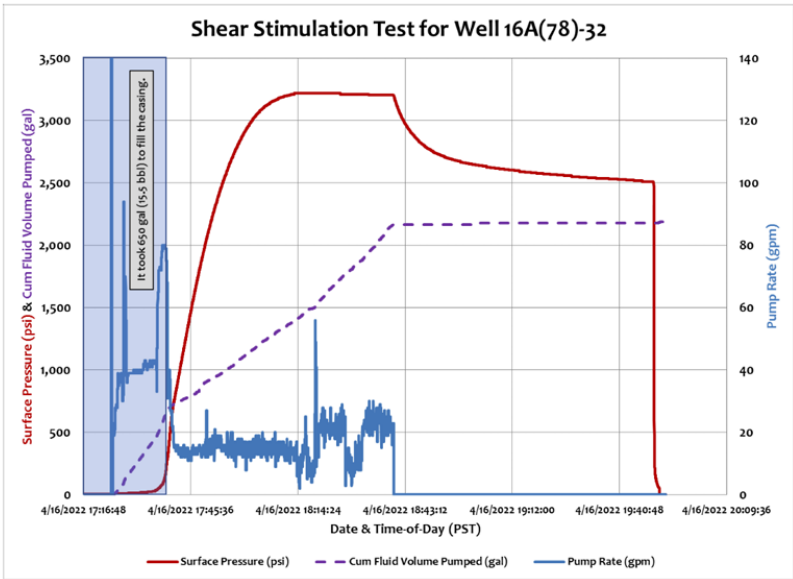

Figure 5: 'Tendency for shear stimulation test' performed prior to the first stage of stimulation during the April 2022 stimulations in 16(A) (figure reproduced from page 22 of Utah FORGE, 2023). Injection rate is very low to maintain pressure below the minimum principal stress. Subsequent testing showed that Shmin was reached around 4000 psi WHP (Utah FORGE, 2023).

As noted by McClure and Horne (2014a), if BHP goes above Shmin, it becomes ambiguous whether shear stimulation or fracture opening/propagation is responsible for stimulation. With BHP slightly below Shmin, Coulomb stress analysis predicts that shear should occur on natural fractures, but fracture opening cannot occur. Thus, the 'tendency for shear stimulation' test at FORGE provides a test for unambiguous evidence of shear stimulation. In this case, the test found little to no evidence of shear stimulation. Similar tests were performed at the EGS Collab project and the Desert Peak project. At EGS Collab, shear stimulation was not observed, despite repeated efforts targeting specific natural fractures along the wells (Kneafsey et al., 2025). In the Desert Peak test, stimulation eventually occurred after days of injection at constant temperature, probably indicating thermally induced stimulation, rather than shear stimulation (Chabora et al., 2012; McClure and Horne, 2014a). Very few historic EGS stimulations have been able to perform stimulation injections at BHP below the minimum principal stress (McClure and Horne, 2014b).

As reviewed by McClure and Horne (2014b), historical data has shown a correlation between the presence of large-scale, well-developed faults and the efficacy of unpropped shear stimulation designs. Consistent with this theory, while a large number of natural fractures were observed in the 16(A), there was not evidence of major, large-scale faulting cutting across the wells (Finnila and Jones, 2024; Jones et al., 2025).

Notwithstanding the comments above, there may be evidence of a small amount of stimulation from the unpropped stimulations. Figure 5 – performed immediately prior to the first-ever stimulation treatment, shows that it was possible to inject at 0.5 bpm with a WHP around 3250 psi. Figure 4 – showing data after the three unpropped simulation stages – shows that it was possible to inject at 2.5 bpm for tens of minutes before WHP reached 3000 psi. While there does seem to be a modest apparent increase in injectivity, this is not necessarily due to 'shear stimulation of natural fractures.' A large number of new perforations were shot from the 16(A) following the first stimulation stage (after the test shown in Figure 5 was performed), creating more connections to the reservoir than were available during the original shear stimulation test. Also, the three proppantless stages of high rate injection were performed at BHP above Shmin, almost certainly propagating opening mode fractures through the formation. These newly formed hydraulic fractures could have closed with slight mismatch in their asperities and retained a modest amount of unpropped conductivity.

2.3 Natural fracture observations from fiber and microseismic

Despite the lack of evidence for shear stimulation, natural fractures do appear to have influenced fracture propagation during the FORGE stimulations. Figure 6 shows crosswell fiber strain rate measurements taken along the 16(B) during stimulation of the 16(A). The early stages show relatively conventional opening mode frac hits signatures, roughly in the locations where they might be expected to occur if vertical planar fractures were propagating from 16(A). However, during Stage 8, there is an unusual signature that probably indicates slip along a fault (Jurick et al., 2025). Figure 7 shows microseismic observations during the stimulations. A relatively large and coherent planar feature is apparent in approximately the same place as the anomalous fiber signature in Stage 8 (Dana Jurick, personally communication).

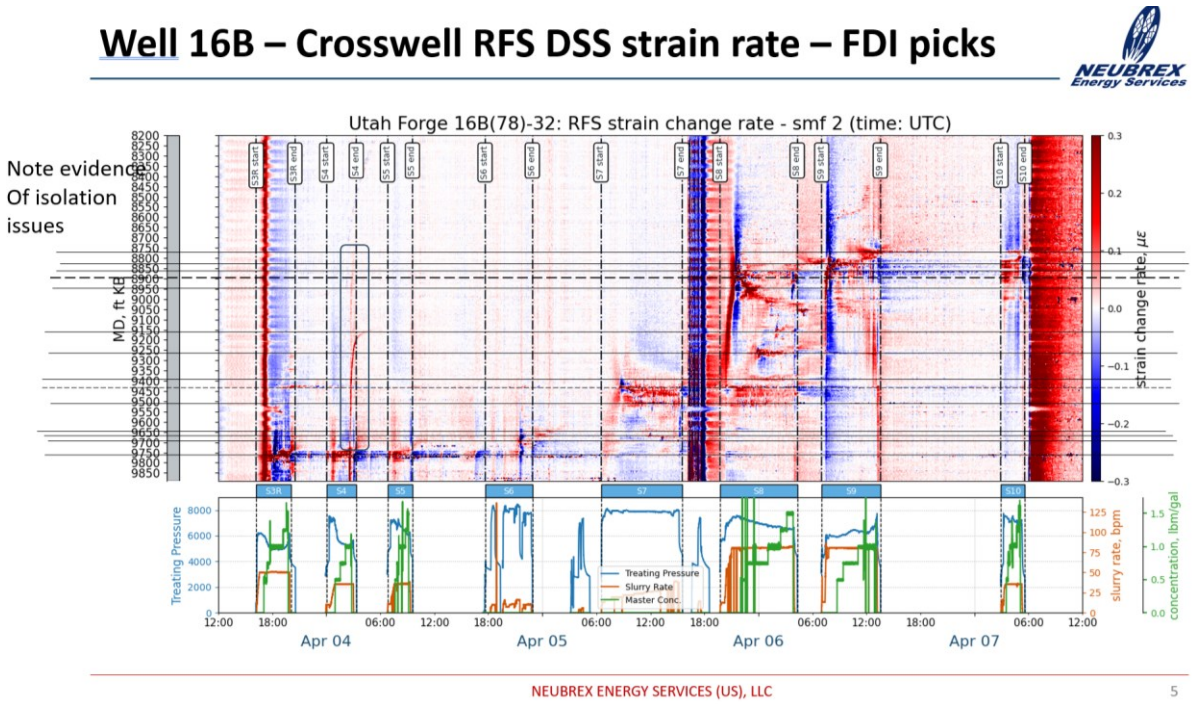

Figure 6: Crosswell fiber measured in Well 16(B) during the March/April 2024 stimulations of 16(A) (figure courtesy of Dana Jurick).

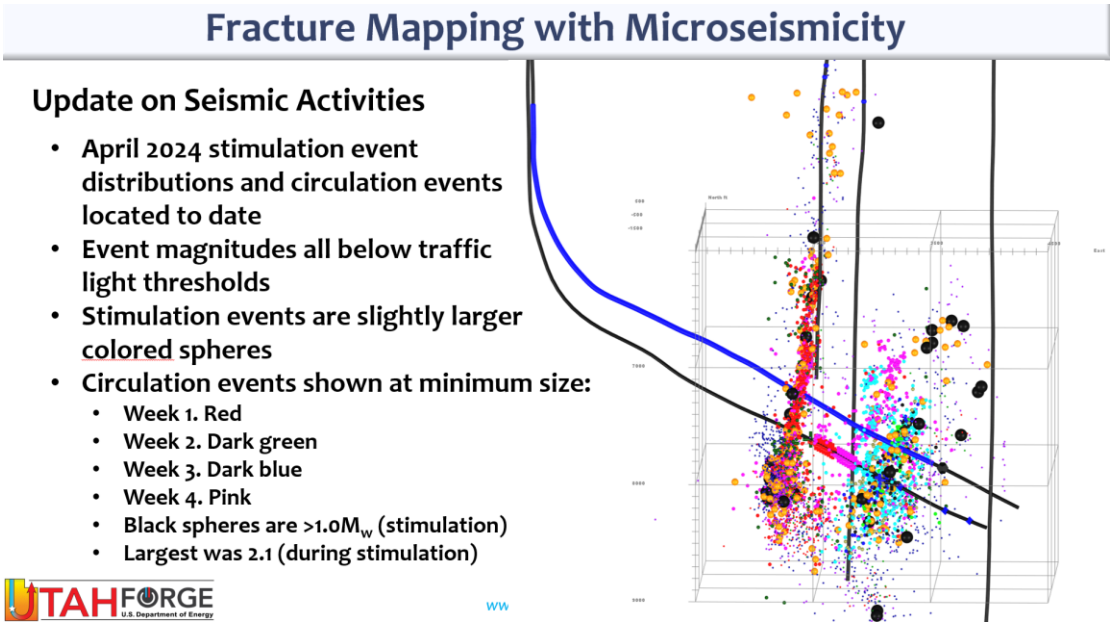

Figure 7: Microseismicity measured during the March/April 2024 stimulations of Wells 16(A) and 16(B) (Utah FORGE, 2024a).

Overall, how should we interpret these observations? A plausible interpretation is that in many stages, opening mode fractures are able to propagate relatively unimpeded through the formation. However, in a minority of stages, they may encounter a sufficiently-developed fault or fractures zone that is able to divert fluid.

It is likely that the preexisting fault/fracture zone was mechanically jacked open and had proppant emplaced into it. 731,000 lbs of proppant were pumped into Stage 8, and this proppant could only have been placed into mechanically open fractures.

2.4 Tracer test results

A variety of tracer tests were run with the 16(A) and 16(B) stimulations and flow tests (Fredd, 2024, 2025; RESMAN, 2025). Fredd (2025) reports that the mean swept volume from the tests was 4680 bbl. This is a surprisingly large swept volume, which is generally positive for our assessment of the heat sweep efficiency between the wells.

Fredd (2025) and RESMAN (2025) provided a detailed analysis of the tracer tests, covering many topics outside the scope of the present work. In this section, I utilize an approach similar to the analysis from Fredd (2024, 2025) to place bounds on the porosity of the propped area. Although similar, the analysis from Fredd (2025) utilized somewhat different assumptions and arrived at some conclusions different from those than reached in this paper.

As discussed in Section 2.2, stimulation was ineffective without proppant. Therefore, we can reasonably assume that the swept pore volume is focused on the areas of the fracture where proppant was placed. From this assumption, we can make a rough estimate for the pore volume of the propped/stimulated fracture area. 3.0 million pounds of proppant were pumped in total from 16A and 16B, which works out to a total volume for the rock matrix (not counting porosity between the grains) of 3265 bbl (Fredd, 2025). Assuming 40% porosity, this should yield a pore volume of:

$$PV = V_p \frac{\phi}{1-\phi} = 3265 \frac{0.4}{1-0.4} = 2178\ bbl \quad (1)$$

Where PV is the pore volume of the propped area, ϕ is porosity, and V_p is the volume of the proppant grains (not including the porosity around them).

We cannot expect that the flow pathway between the wells will sweep 100% of the propped volume. Some proppant will enter dead-end fractures that do not connect between the wells, and some proppant will settle below the 16(A) well, or be placed above the 16(B) well. Thus, if we hypothesize that 50% of the propped volume participates in a flow pathway between the wells, then we can calculate that the swept volume should be 2178/2 = 1088 bbl. However, the actual value of 4680 bbl is 4.3x larger than what we might have expected, and 2.15x larger than the maximum value that we could have expected, assuming a 40% porosity. Why is there a mismatch?

One possibility is that natural fractures are participating in the flow pathways between the wells, and the tracers are partially sweeping through this additional pore volume. While unpropped stimulations were ineffective, we cannot rule that small-scale natural fractures or the fault/fracture zone seen in fiber and microseismic during Stage 8 could be contributing pore volume.

A second possibility is that the porosity of the propped fracture surface area is higher than we initially hypothesized. If we have measured the mean swept volume of the flowing tracer pathway, V_{swept}, and we assume that it sweeps through a certain fraction of the proppant pack as the flowing pathway, *eff*, then we can solve Equation 1 to write:

$$\phi = \frac{V_{swept}}{eff * V_p + V_{swept}} \quad (2)$$

If we assume that *eff* is 0.5, then we can calculate:

$$\phi = \frac{V_{swept}}{eff * V_p + V_{swept}} = \frac{4680}{0.5*3265+4680} = 74\% \quad (3)$$

Is this number plausible? If the fractures are filled with a packed bed of particles, then no, it is not possible to have 74% porosity. However, if the proppant is distributed in a thinly dispersed monolayer, then such high porosity can be possible. For example, Figure 12 from Elsarawy and Nasr-El-Din (2019) shows a laboratory measurement of 63% in a fracture with proppant monolayer at 0.2 lbs/ft^2. A schematic of this phenomenon can be seen in Figure 9 from Fredd et al. (2001).

To create a monolayer-type distribution of proppant, the amount of proppant per area must be less than roughly 0.25 lbs/ft^2 (with the exact amount depending on grain size). In fact, numerical modeling calibrations to field-scale diagnostics in shale do typically suggest that proppant is distributed across the propped area at an average concentration in a range of 0.05-0.25 lbs/ft^2 (Fowler et al., 2020; McClure et al., 2020; Singh et al., 2025). Thus, we can conclude that the surprisingly high values of apparent porosity are physically plausible and consistent with field experience, at least in shale.

How much fracture surface area does the swept volume of 4680 bbl correspond to? If we assume a porosity of 74%, then 0.15 lbs/ft^2 corresponds to an aperture of 0.044 inches. We can then estimate that the swept area is:

$$A = \frac{PV}{W} * \frac{1}{\phi} = 4680 * 5.615 * \frac{12}{0.044} * \frac{1}{.74} = 9.7e6\ ft\text{^}2 \quad (4)$$

For reference, utilizing a similar, but somewhat different, set of assumptions, Fredd (2025) estimated a swept fracture surface area of 5.5e6 ft^2.

The wells are roughly 330 ft apart vertically. If we assume that fluid flowed out laterally with a width of 300 ft, then there should be roughly 1e5 ft^2 per flowing fracture between the wells. Thus, if the swept area crosses 9.6e6 ft^2, this would correspond to 96 flowing fractures. This is a surprisingly high number because there were only 27 perforation clusters stimulated along 16(A), and some of these

did not break down. Nevertheless, this is not impossible because core-through studies in shale consistently observe more hydraulic fracture strands than perforation clusters (Raterman et al., 2017; 2019; Ugueto et al., 2021; Ciezobka and Maity, 2022; Brinkley et al., 2023).

These are merely back-of-the-envelope calculations. Plausible numbers are being applied, but if we made slightly different assumptions, such as using different values of *W* or *eff*, then different values could be reached. Nevertheless, it is reassuring that if we plug reasonable values into the governing equations, the calculations suggest that a substantial fracture surface area is participating in the flow pathway.

What would a 'bad' swept volume have looked like? Generally, lower swept volume implies lower fracture surface area. For example, if there was only a single fracture connecting the wells, with area of 1e5 ft^2, porosity of 34%, and aperture of 0.09 inches, then the swept volume would have been 45 bbl. The actual swept volume was 100x greater than it would have been under this pessimistic scenario.

3. CRITICAL ANALYSIS OF ALTERNATIVE INTERPRETATIONS

3.1 Shear stimulation

3.1.1 Minifrac tests in the Well 58-32

Wang et al. (2024) perform a modeling study on multiple cycle minifrac tests performed in the vertical Well 58–32, which was drilled as a pilot hole at the FORGE project in 2017. The Wang et al. (2024) model neglects the processes of fracture jacking and/or propagation and assumes that changes in injectivity are caused exclusively by shear stimulation of natural fractures. Is this assumption supported by the data? Is there a way to differentiate between shear stimulation and fracture opening?

Injection was performed into a 46 m openhole section at the bottom of the Well 58-32. Figure 6 from Wang et al. (2024) shows that eight injection cycles were performed. Five of the eight cycles were performed at low rate (1-2 kg/s), and three of the cycles were performed at high rate (16-27 kg/s). Figure 16 from Wang et al. (2024) shows pressure versus time during Cycles 5-8, which encompasses the three high-rate injections.

Shear stimulation of natural fractures is capable of causing an abrupt increase in injectivity, causing injection pressure to flatten at a threshold pressure (Figure 3-13 from McClure, 2012). However, shear stimulation is an *irreversible* process. It persists after shut-in, and it does not reoccur at the same threshold pressure during a second repressurization cycle. Therefore, if repeated injection cycles are performed, we can differentiate between shear stimulation and fracture reopening/jacking by observing the pressure response in the cycles after the first cycle (Section 4.2.3 from White et al., 2017). With the shear stimulation hypothesis, the first cycle may exhibit an abrupt flattening of injection pressure as stimulation occurs. However, during subsequent cycles, a different response should occur. There should be a more gradual pressure increase, with no sudden flattening, because fracture slip and 'stimulation' has already occurred. The fracture cannot slip again unless a significantly larger volume of fluid and/or higher pressure are used. On the other hand, with fracture opening and closure, the process is reversible, and rapid pressure increase, followed by abrupt flattening, will be seen consistently in every cycle.

Figure 16 from Wang et al. (2024) shows that in the actual data, pressure increases rapidly and abruptly flattens at a threshold pressure in each high-rate cycle. This observation is consistent with fracture opening. The simulation results from Wang et al. (2024) – which assume shear stimulation only – do not reproduce the abrupt flattening at every cycle. Instead, they show – as expected for a shear stimulation model – gradual increases in injection pressure in the second and third high-rate cycles. Also, the simulation results consistently overestimate the rate that pressure falls off after shut-in. This is a consequence of the shear stimulation assumption – because it uses shear stimulation, the model assumes that stimulation persists after pressure falls off and overestimates the fracture conductivity after shut-in. Conversely, a model with fracture reopening/closure would have reversible drop in fracture conductivity after shut-in, reducing the rate of pressure falloff.

Overall, the *inability* of the simulation to match the data shown in Figure 16 from Wang et al. (2024) helps to *falsify* the hypothesis of pure shear stimulation. Instead, the data shows reversible and abrupt increase/decrease in injectivity at a threshold pressure over multiple cycles. These observations are consistent with fracture opening/closure, and they are inconsistent with the shear stimulation hypothesis.

The approach used by Wang et al. (2024) is not unusual in EGS modeling. As reviewed by McClure and Horne (2014b), a large majority of EGS models from the 1990s to 2010s neglected the possibility of hydraulic fracture propagation, even though nearly every EGS project on record has injected with bottomhole pressure greater than the minimum principal stress.

3.2 Estimating 'formation permeability' from microseismic

Elsworth (2024) proposes to estimate the formation permeability from the rate that microseismicity propagated from the wells during the stimulation of 16(A). This procedure is based on the assumption that pressure increase around the injector can be modeled as if it is flow through a porous media, based on the classical equation for 'radius of investigation' (Shapiro et al., 1997):

$$r_{inv} = \sqrt{4\pi D t} = \sqrt{\frac{4\pi k}{c_t \phi \mu} t} \tag{5}$$

This procedure neglects the possibility of fracture opening and propagation. Hydraulic fracture propagation is a fundamentally different process than flow through porous media. Unlike single-phase flow through porous media, fracture propagation is not governed by the

diffusivity equation. Hydraulic fractures can open and propagate *even if the permeability is zero*. In fact, higher permeability results in *slower* fracture propagation because it causes more leakoff (Equations 9.41 and 9.42 from Valko and Economides, 1995).

Therefore, it is not valid to apply Equation 5 to estimate formation permeability during injection when the bottomhole pressure exceeds the minimum principal stress. Microseismicity spreads from the well as fluid leaks off from opening and propagating hydraulic fractures and/or reopening natural fractures.

Equation 5 will not be directionally correct in predicting the impact of formation properties on the rate that microseismicity propagates from the well. It predicts that higher formation permeability will result in microseismicity spreading more rapidly from the well; but if microseismicity is driven by leakoff from hydraulic fractures, the opposite will hold true – greater formation permeability will reduce the rate of hydraulic fracture propagation and the rate that microseismicity spreads from the well.

Finally, it is not valid to interpret Equation 5 as representing an estimate for the permeability of the propagating hydraulic fracture. Fracture propagation is a different physical phenomenon than flow through porous media, and it cannot be described with equations based on the diffusivity equation (Valko and Economides, 1995).

3.3 Tracer interpretations

3.3.1 Overview

Reviewing the tracer test analyses presented by Fredd (2024, 2025), there were several areas where I would have drawn different conclusions. However, their analysis is still in-progress, and the results are not finalized. Therefore, I will defer providing a detailed commentary on their conclusions until they are available in a written report.

In the sections below, I provide general analysis of the tracer results presented by Fredd (2024, 2025).

3.3.2 Circulation volume efficiency

Fredd (2025) define the term 'circulation volume efficiency' as the volume of the swept path of a tracer slug test divided by the volume of fluid injected. As per Fredd (2025), the mean swept volume of the tracer test between 16(A) and 16(B) was 4680 bbl. The total volume of slurry injected during the stimulations of the two wells was in the ballpark of 123,000 bbl, yielding a 'circulation volume efficiency' metric of 4%.

This metric is presented solely as a "high-level metric to compare the overall well pattern and design from project to project" (Chris Fredd, personal communication). However, it is interesting to note that the 'circulation volume efficiency' does have a relationship with the percentage of the fracture surface area that is swept by flow, as we can briefly derive.

From mass balance (and neglecting the compressibility of the injection fluid), we can write that at the completion of injection:

$$V_{inj} = W_{inj}A + V_{inj}V_{frac,leakoff} \rightarrow A = \frac{V_{inj}(1-V_{frac,leakoff})}{W_{inj}} \quad (6)$$

Where $V_{frac,leakoff}$ is the fraction of fluid that has leaked off at shut-in, V_{inj} is the total volume of slurry injected (including both fluid and proppant volume), W_{inj} is the average fracture aperture at the end of injection, and A is the total fracture surface area (for simplicity, the equation neglects any continued propagation after shut-in).

As defined by Fredd (2025), the 'circulation volume efficiency,' eff_{circ}, is:

$$eff_{circ} = \frac{V_{swept}}{V_{inj}} \quad (7)$$

Where V_{swept} is the mean swept volume from the tracer test. Note that V_{inj} refers to a volume of slurry, while V_{swept} refers to a pore volume. Because the volume fraction of proppant in the injected fluid was low in these stimulations, the distinction makes a minimal difference. We can write that $V_{swept} = V_{swept,bulk}\phi_{swept}$, where $V_{swept,bulk}$ is the total volume of the swept fracture volume during circulation (including the volume occupied by proppant), and ϕ_{swept} is the porosity of the swept fracture volume during. Further, let's define that $A_{frac,swept}$ is the fraction of the total fracture area that is swept by the main flow pathway during tracer test. Therefore:

$$V_{swept,bulk} = W_{inj}W_{frac}A_{frac,swept}A \quad (8)$$

Where W_{frac} is the fraction of the total aperture during pumping that is retained after shut-in and fracture closure.

Combining these equations:

$$eff_{circ} = \frac{V_{swept}}{V_{inj}} = \frac{W_{inj}W_{frac}\phi_{swept}A_{frac,swept}A}{V_{inj}} = \frac{W_{inj}W_{frac}\phi_{swept}A_{frac,swept}}{V_{inj}}\frac{V_{inj}(1-V_{frac,leakoff})}{W_{inj}} = A_{frac,swept}\left(1-V_{frac,leakoff}\right)W_{frac}\phi_{swept} \quad (9)$$

From Equation 9, we see that if there is no leakoff and if the aperture during circulation was equal to the aperture during stimulation, then the 'circulation volume efficiency' will be equal to the fraction of total area that is swept multiplied by the porosity of the swept area.

If we assume 30% leakoff, that 15% of the aperture is retained after shut-in, and that the porosity is 50%, then we can calculate that even if $A_{frac,swept}$ was 100%, then the value of circulation volume efficiency would be 5.25%. Conversely, since the actual observed value was 4%, we could use these numbers to estimate $A_{frac,swept}$ to be 74%. However, this number is implausibly high. As noted by Fredd (2024, 2025), the microsesimic cloud is much larger than the well-spacing, suggesting that there is a substantial percentage of the created fracture area that must be outside the flow path.

Why does this calculation yield a value of $A_{frac,swept}$ that seems too high? As discussed in Section 2.4, calculations suggest that the porosity of the proppant pack is probably high, which suggests that the proppant is placed sparsely in fractures with relatively low aperture. Perhaps it would be more reasonable to assume that W_{frac} is 0.5, and that ϕ_{swept} is 0.74. In that case, along with assuming 30% leakoff, we would calculate that a value of eff_{circ} of 4% implies that $A_{frac,swept}$ is 15%. This number is more 'in the ballpark' of what we might have estimated from consideration of the well configuration and the microseismic fracture geometry. For reference, Fredd (2024, 2025) compared the well geometry with the shape of the microseismic cloud and estimates of swept area from the tracer test and estimated that 22% of the created fracture surface area must be part of the flow pathway.

Clearly, there are significant uncertainties in the inputs to Equation 9. With different assumptions, we could arrive at significantly different predictions for $A_{frac,swept}$. But for any plausible set of inputs, the calculations suggest that the value of $A_{frac,swept}$, the fraction of total area swept by the flow path, is much greater than the 'circulation volume efficiency.'

Experience from slickwater fracturing in shale suggests that a large percentage of the total fracture area is likely to be unpropped (Liang et al., 2022). Therefore, if we assume that the swept area is confined to the propped area (because of the ineffectiveness of unpropped stimulations), then the fraction of the propped area that is swept by the flow pathway must be substantially larger than the fraction of the total fracture area that is swept by the flow pathway. For example, plausible numbers would be that $A_{frac,swept}$ is 15%, while the percentage of total area that is propped is 30%, and the fraction of propped area in the flow pathway is 50%.

It may seem inefficient to leave such a large fraction of the fracture surface area unpropped. Nevertheless, this is the norm for fracture design in shale, where most fracturing is done with low viscosity fluids. Thicker fluids and smaller fluid volumes can be used to prop a greater fraction of the total fracture area. However, these approaches have drawbacks: (a) conductivity damage from incomplete gel cleanout, (b) greater chemical cost, (c) limitations on injection rate that affect perforation pressure drop and stage length, and (d) they likely result in greater placed proppant concentration, which may actually *reduce* propped area (as discussed in Section 3.3.3). So, while thicker fracturing fluids for EGS are worth consideration, we must be aware that there are engineering pros and cons to the different options.

3.3.3 Comparing swept volume with the injected proppant mass

As discussed in Section 2.4, the swept tracer volume is significantly larger than we might have expected from consideration of the volume of proppant pumped. This is probably caused by elevated porosity in the propped fracture area, because the proppant is distributed at low concentration. Natural fracture porosity may also contribute.

Proppant grains at low concentration are only able to 'hold open' fracture area within a distance of mm to cm. Thus, to the extent that there are unpropped areas 'held open' by the proppant, these unpropped areas must exist in very close proximity to where the proppant is placed. Otherwise, the unpropped areas would close off and have low conductivity (since unpropped stimulations at FORGE had low efficacy).

If there are intermixed regions with and without proppant at the scale of mm-cm, what are the implications for heat sweep efficiency?

Guo et al. (2016) performed a simulation study on the effect of heterogeneity on heat sweep efficiency. They found that when the spatial correlation length of heterogeneity is high, then it has a significantly negative effect on heat sweep efficiency. However, when the spatial correlation length is small – representing small-scale heterogeneity that is not coherent at large scale – then heterogeneity has a minor effect. In the case of thinly placed monolayer-type proppant placement, variations between propped and unpropped area must inherently be very small. Thus, this type of small-scale heterogeneity will not have a significantly negative effect on heat sweep efficiency. If there had been coherent large-scale heterogeneity, this would have manifested as a surprisingly low swept tracer volume, because the spatially coherent short-circuit pathways would have dominated the tracer return curve.

Overall, low proppant concentration within the propped area is highly desirable. Proppant mass is a significant driver of cost. For a specified volume of proppant injected V_p (solely the volume of the solid grains, not counting the porosity between them), then propped surface area will be:

$$A_{propped} = \frac{V_p}{1-\phi} \frac{1}{W} \quad (9)$$

Where W is width and ϕ is porosity. Thus, we see that if the porosity of the propped area is greater, or if the width of the propped area is lower, then for a specified volume of proppant injected, the total propped fracture surface area will be greater. In other words, a high porosity monolayer-like distribution of proppant (low W and high ϕ) is the most economically efficient way to generate maximum

stimulated area at minimum proppant cost. Although, for some sufficiently high value of ϕ within the proppant pack, the fracture will have insufficient conductivity because of the low proppant concentration.

3.3.4 Gravitational settling of proppant

Proppant settling to the bottom of the fracture is inhibited by fracture roughness (Huang et al, 2020; McClure et al., 2020; Ciezobka and Maity, 2022). Ciezobka and Maity (2022) refer to this process as 'localized screenout.' McClure et al. (2020) calls it 'proppant trapping' or 'proppant immobilization.' The concept of a proppant bed at the bottom of the fracture – with an unpropped region above it – dates back to the early days of hydraulic fracturing (Kern et al., 1959). However, in low permeability formations such as shale, an alternative concept is that proppant is placed in a relatively low concentration, as a monolayer and/or with patchy placement, across much of the fracture height, and prevented from fully settling out by fracture roughness. This concept can explain why wells with slickwater fracturing treatments are routinely able to drain from rock 100s of ft above (Bachleda et al., 2024; Ge et al., 2024).

The FORGE dataset appears to be an excellent example of this phenomenon. Unpropped stimulations were ineffective. Then, stages stimulated with low concentration proppant were able to connect flow at high rate between wells with 330 ft of vertical separation. These results could only be possible if a large amount of propped and stimulated fracture surface area was placed across the hundreds of feet above the 16(A).

4. CONCLUSIONS

2024 was a very successful year for the FORGE project, both operationally and scientifically. The project was able to achieve a 26 kg/s circulation rate across only 1000 ft of stimulated lateral. Production logs indicate that flow was reasonably well-distributed across the lateral, although not with as much uniformity as would be ideal. Nonuniformity may have been increased by the variety of frac designs employed across the lateral, as well as operational issues that could be addressed in future projects, such as limitations on the maximum injection wellhead pressure. On the other hand, it is clear that geologic variability – such as the intermixing between granitic and gneissic lithology – was responsible for much of the variability. Fiber and microseismic data indicate that a preexisting fault or fracture zone likely captured the fractures from one or more stages, affecting propagation direction and fracture morphology.

Comparison of propped and unpropped stimulations demonstrates a stark difference. Stimulation stages with proppant were much more effective. Injection at BHP slightly below Shmin – high enough to supposedly cause slip but not high enough to jack open fractures – resulted in little or no apparent stimulation or microseismicity. The results demonstrate that fracture opening and/or propagation was widespread during the stimulations, and that unpropped natural fracture permeability and the formation's ability to shear stimulate was limited.

Crosswell tracer results indicate a substantially larger swept volume that might have been expected based on the volume of proppant that was pumped. This indicates that either: (a) porosity from natural fracture pathways elevated the swept volume (notwithstanding the lack of evidence for shear stimulation seen in the injection data), or (b) the proppant pack porosity is very high, because the proppant is distributed in a low concentration, monolayer-like distribution. While there is uncertainty in quantitative interpretation of reservoir parameters from tracer results, the qualitative implication is that circulating fluid is passing through a stimulated fracture surface area that is as-high or higher than could have been expected from the volume of proppant that was pumped.

REFERENCES

Bachleda, Jana, Ruben Cisneros, Dan Carson, Helm Donahue, Michael Manigold, Muqing Jin, Shuangyu Ge, Jiang Wu, and Faye Liu. 2024. Optimizing Infill Development in the Delaware Basin Through Integration of Geochemistry, Tracer, Pre-Frac Step Down Test, and Pressure Data. Paper presented at the Unconventional Resources Technology Conference, Houston, TX.

Baria R., Michelet, S., Baumgärtner, J., Dyer, B., Gerard, A., Nicholls, J., Hettkamp, T., Teza, D., Soma, N., Asanuma, H., Garnish, J., and Megel, T. 2004. Microseismic monitoring of the world's largest potential HDR reservoir. Proceedings of the Twenty-Ninth Workshop on Geothermal Reservoir Engineering. Stanford University.

Brinkley, Kourtney, Cameron Thompson, Jackson Haffener, Sarah White, Chris Ketter, Jarret Borell, Joe Comisky, Eric Hart, Kyle Haustveit, Matthew Herrin, Peter Jones, Kevin Pelton, Ken Pfau, Buddy Price, Jon Roberts, and Molly Turko. 2023. Redefining Recoverable Reserves in the Eagle Ford: Refracs and Infill Development Lessons Learned from the Hydraulic Fracturing Test Site 1 (HFTS) Phase 3. Paper SPE-212340-MS presented at the Hydraulic Fracturing Technology Conference, The Woodlands, TX.

Chabora, E., E. Zemach, P. Spielman, P. Drakos, S. Hickman, S. Lutz, et al. 2012. Hydraulic stimulation of Well 27-15, Desert Peak Geothermal Field, Nevada, USA. Paper presented at the Thirty-Seventh Workshop on Geothermal Reservoir Engineering, Stanford University.

Ciezobka, Jordan, and Debotyam Maity. 2022. HFTS-2 Final Report. GTI Energy Project Number 22315. Prepared for the US Department of Energy.

Elsarawy, Ahmed, M., and Hisham A. Nasr-El-Din. 2019. A new method to measured propped fracture width and proppant porosity in shale fractures. Journal of Petroleum Science and Engineering **181**(106162).

Elsworth, Derek. 2024. Utah FORGE 5-2419: Seismicity-Permeability Relationships Probed via Nonlinear Acoustic Imaging - 2024 Annual Workshop Presentation. https://gdr.openei.org/submissions/1642.

England, Kevin. 2024. Review of the 2024 Stimulation Program at Utah FORGE. Hydraulic Fracturing Seminar Series, American Rock Mechanics Association Hydraulic Fracturing Community. https://www.youtube.com/watch?feature=shared&v=wFe0DVhcHak.

England, Kevin, PeiJian Li, Pengju Xing, Joseph Moore, and John McLennan. 2025. 2024 Enhanced Geothermal Hydraulic Fracturing Campaign at Utah FORGE. Paper SPE-223519-MS presented at the Hydraulic Fracturing Technology Conference and Exhibition, The Woodlands, TX.

Evans, Keith F., Albert Genter, Judith Sausse. 2005. Permeability creation and damage due to massive fluid injections into granite at 3.5 km at Soultz: 1. Borehole observations. Journal of Geophysical Research, **110**(B04203).

Finnila, Aleta, and Clay Jones. 2024. Updated Reference Discrete Fracture Network Model at Utah FORGE. Paper presented at the 49th Workshop on Geothermal Reservoir Engineering, Stanford University.

Fowler, Garrett, Mark McClure, and Craig Cipolla. 2020. Making sense out of a complicated parent/child well dataset: A Bakken case study. Paper SPE-201566-MS presented at the Annual Technical Conference Exhibition, Houston, TX. https://doi.org/10.2118/201566-MS.

Fredd, C. N., S. B. McConnell, C. L. Boney, and K. W. England. 2001. Experimental Study of Fracture Conductivity for Water-Fracturing and Conventional Fracturing Applications. SPE Journal, **6**(03): 288-298.

Fredd, Chris. 2024. Utah FORGE – Seeing is Believing with Advanced Tracer Interpretation. Bimonthly Utah FORGE Webinar, November 6, 2024.

Fredd, Chris. 2025. GEODE Series - Webinar: Advanced Tracer Interpretation at Utah FORGE Provides New Insights on Completion and Stimulation Challenges for Enhanced Geothermal System. January 17, 2025. https://streaming.spe.org/geode-series-advanced-tracer-interpretation-at-utah-forge-provides-new-insights-on-completion-and-stimulation-challenges-for-enhanced-geothermal-system-2.

Ge, Shuangyu, Jana Bachleda, Luke Fidler, Josh Sigler, Tao Lv and Faye Liu. 2024. Statistics and Case Studies of Drainage Frac Height and Zonal Contribution of Stacked Plays in the Midland and Uinta Basin. Paper SPE-217764-MS presented at the Hydraulic Fracturing Technology Conference, The Woodlands, TX.

Glauser, Walter, John McLennan, and Ian Walton. 2013. Do perforated completions have value for engineered geothermal systems. In Effective and Sustainable Hydraulic Fracturing, ed. Andrew P. Bunger, John McLennan and Rob Jeffrey, 95-121. InTech.

Guo, Bin, Pengcheng Fu, Yue Hao, Catherine A. Peters, Charles R. Carrigan. 2016. Thermal drawdown-induced flow channeling in a single fracture in EGS. Geothermics, **61**: 46-62.

Huang, Hai, Tayfun Babadagli, Huazhou Li, Kayhan Develi, Desheng Zhou. 2020. A visual experimental study on proppants transport in rough vertical fractures. International Journal of Rock Mechanics and Mining Science, **134**(104446).

Jones, Clay G., Stuart S. Simmons, and Joseph N. Moore. 2025. Characterization of Drill Core from Hydraulically Stimulated Crystalline Rock Following Hydraulic Fracturing at the Utah FORGE Geothermal Test Site. 2025. Paper presented at the 50th Workshop on Geothermal Reservoir Engineering. Stanford University.

Jurick, Dana, Alan Reynolds, and Mukul M. Sharma. 2025. Improving the Connectivity between Injection and Production Wells in Enhanced Geothermal Systems using Fiber Optic Data. SPE Hydraulic Fracturing Technology Conference and Exhibition. Paper SPE-223456-MS presented at the Hydraulic Fracturing Technology Conference and Exhibition, The Woodlands, TX.

Kern, L. R., T. K. Perkins, R. E. Wyant. 1959. The Mechanics of Sand Movement in Fracturing. Journal of Petroleum Technology 11 (7): 55-57. http://dx.doi.org/10.2118/1108-G.

Kneafsey, Tim, et al. 2025. The EGS Collab Project: Outcomes and Lessons Learned from Hydraulic Fracture Stimulations in Crystalline Rock at 1.25 and 1.5 km depth. Geothermics **126**(103178).

Liang, Yueming, Holger Meier, Karthik Srinivasan, Hussain Tahir, Alberto Ortega, Kelvin Amalokwu, James Friedrich, Joy Okpala, Kendal Decker, Matthew Brown, Tim Benish, Haylee Crozier, Peeyush Bhargava, Prasad Sumant, and James Reavis. 2022. Accelerating Development Optimization in the Bakken Using an Integrated Fracture Diagnostic Pilot. Paper presented at the SPE/AAPG/SEG Unconventional Resources Technology Conference, Houston, TX.

McClure, Mark W. 2012. Modeling and characterization of hydraulic stimulation and induced seismicity in geothermal and shale gas reservoirs. PhD thesis. Stanford University.

McClure, Mark W., and Roland N. Horne. 2014a. An Investigation of Stimulation Mechanism in Enhanced Geothermal Systems. International Journal for Rock Mechanics and Mining Sciences **72**: 242-260.

McClure, Mark, and Roland Horne. 2014b. Characterizing hydraulic fracturing with a tendency-for-shear-stimulation test. SPE Reservoir Evaluation & Engineering, **17**: 233-243.

McClure, Mark. Matteo Picone, Garrett Fowler, Dave Ratcliff, Charles Kang, Soma Medam, and Joe Frantz. 2020. Nuances and frequently asked questions in field-scale hydraulic fracture modeling. Paper SPE-199726-MS presented at the SPE Hydraulic Fracturing Technology Conference and Exhibition, The Woodlands, TX.

Moore, Joseph, John McLennan, Kristine Pankow, Robert Podgorney, James Rutledge, Peter Meir, Ben Dyer, Dimitrios Karvounis, Falko Bethmann, Pengju Xing, Benjamin Barker, Clay Jones, Stuart Simmons, Branko Damjanac, and Aleta Finnila. 2023. Current Activities at the Utah Frontier Observatory for Research in Geothermal Energy (FORGE). Proceedings, World Geothermal Congress, Beijing, China.

Norbeck, J. H., and Latimer, T. M. 2023. Commercial-scale demonstration of a first-of-a-kind enhanced geothermal system. https://eartharxiv.org/repository/view/5704/.

Norbeck, Jack Hunter, Christian Gradl, and Timothy Latimer. 2024. Deployment of Enhanced Geothermal System technology leads to rapid cost reductions and performance improvements. https://eartharxiv.org/repository/view/7665/.

Raterman, Kevin T., Helen E. Farrell, Oscar S. Mora, Aaron L. Janssen, Gustavo A. Gomez, Seth Busetti, Jamie McEwen, Michael Davidson, Kyle Friehauf, James Rutherford, Ray Reid, Ge Jin, Baishali Roy, and Mark Warren. 2017. Sampling a Stimulated Rock Volume: An Eagle Ford Example. Paper presented at the Unconventional Resources Technology Conference, Austin, TX.

Raterman, K., Liu, Y. and Warren, L. 2019. Analysis of a Drained Rock Volume: An Eagle Ford Example. Paper URTeC-2019-263 presented at the Unconventional Resources Conference, Denver, Colorado. https://doi.org/10.15530/urtec-2019-263.

RESMAN Energy Technologies. 2025. Utah FORGE: RESMAN Well 16A(78)-32 and 16B(78)-32 Stimulation and Circulation Tracer Test Results – 2024. https://gdr.openei.org/submissions/1703.

Shapiro, Sergei, Ernst Huenges, and Gunter Borm. 1997. Estimating the crust permeability from fluid-injection-induced seismic emission at the KTB site. Geophysical Journal International, **131**: F15-F18.

Shiozawa, Sogo, and Mark McClure. 2014. EGS Designs with Horizontal Wells, Multiple Stages, and Proppant. Proceedings of the Thirty-Ninth Workshop on Geothermal Reservoir Engineering, Stanford, CA.

Singh, Ankush, Mohsen Babazadeh, Craig Cipolla, Karan Dhuldhoya, Arjang Gandomkar, John Lassek, Ripu Manchanda, Michael McKimmy, Daniel Ramirez-Tamayo, Reza Safari, Mojtaba Shahri, Steve Smith, and Mark McClure. 2025. Far-field Drainage along Hydraulic Fractures: Insights from Integrated Modeling Studies in the Bakken and Permian Basin. Paper SPE-223567-MS presented at the Hydraulic Fracturing Technology Conference, The Woodlands, TX.

Tenma, Norio, Tsutomu Yamaguchi, George Zyvoloski. 2008. The Hijiori Hot Dry Rock Test Site, Japan Evaluation and Optimization of Heat Extraction from a Two-Layered Reservoir. Geothermics, **37**: 19-52.

Tester J, ed. 2006. The future of geothermal energy: impact of Enhanced Geothermal Systems (EGS) on the United States in the 21st century. Massachusetts Institute of Technology.

Ugueto, Gustavo A., Magdalena Wojtaszek, Paul T. Huckabee, Alexei A. Savitski, Artur Guzik, Ge Jin, J. Andres Chavarria, Kyle Haustveit. 2021. An integrated view of hydraulic induced fracture geometry in Hydraulic Fracture Test Site 2. Paper presented at the SPE/AAPG/SEG Unconventional Resources Technology Conference, Houston, TX.

Utah FORGE. 2023. Phase 3B Year 1 Annual Report: Enhanced Geothermal System Testing and Development at the Milford, Utah FORGE site. Prepared for the US Department of Energy, Contract DE-EE0007080. https://gdr.openei.org/submissions/1523.

Utah FORGE. 2024a. Phase 3B Year 2 Annual Report: Enhanced Geothermal System Testing and Development at the Milford, Utah FORGE site. Prepared for the US Department of Energy, Contract DE-EE0007080. https://gdr.openei.org/submissions/1707.

Utah FORGE. 2024b. Utah FORGE: injection and production test results and reports from August 2024. Energy and Geoscience Institute at the University of Utah. https://gdr.openei.org/submissions/1668.

Valko, Peter, and Michael J. Economides. 1995. Hydraulic Fracture Mechanics. Wiley.

Weddle, Paul, Larry Griffin, and C. Mark Pearson. 2018. Mining the Bakken II – Pushing the envelope with extreme limited entry perforating. Paper SPE 189880-MS presented at the SPE Hydraulic Fracturing Technology Conference & Exhibition, The Woodlands, TX.

White, Mark, Pengcheng Fu, Mark McClure, George Danko, Derek Elsworth, Eric Sonnenthal, Sharad Kelkar, and Robert Podgorney. 2017. A suite of benchmark and challenge problems for enhanced geothermal systems. Geomechanics and Geophysics for Geo-Energy and Geo-Resources, **4**:79–117.

Xing, Pengju, Kevin England, Joseph Moore, Robert Podgorney, and John McLennan. 2024. Analysis of Circulation Tests and Well Connection at Utah FORGE. Paper presented at the 49th Workshop on Geothermal Reservoir Engineering, Stanford University.

Wang, Yu, Yilong Yuan, Bing Guo, Hongwu Lei, Huixing Zhu, Hailong Tian, and Tianfu Xu. 2024. Numerical simulation of hydro-shearing stimulation in the enhanced geothermal system at the Utah FORGE site. Engineering Geology, **343**(107823).

Zoback, M. D. 2007. Reservoir Geomechanics, Cambridge University Press, Cambridge.